



Full length article

9R phase enabled superior radiation stability of nanotwinned Cu alloys via *in situ* radiation at elevated temperatureCuncai Fan^a, Dongyue Xie^b, Jin Li^a, Zhongxia Shang^a, Youxing Chen^c, Sichuang Xue^a, Jian Wang^b, Meimei Li^d, Anter El-Azab^{a,e}, Haiyan Wang^{a,f}, Xinghang Zhang^{a,*}^a School of Materials Engineering, Purdue University, West Lafayette, IN, 47907, USA^b Nebraska Center for Materials and Nanoscience, University of Nebraska-Lincoln, Lincoln, NE, 68583-0857, USA^c Department of Mechanical Engineering and Engineering Science, University of North Carolina, Charlotte, NC, 28223-0001, USA^d Nuclear Engineering Division, Argonne National Laboratory, Argonne, IL, 60439, USA^e School of Nuclear Engineering, Purdue University, West Lafayette, IN, 47907, USA^f School of Electrical and Computer Engineering, West Lafayette, IN, 47907, USA

ARTICLE INFO

Article history:

Received 22 September 2018

Received in revised form

9 January 2019

Accepted 23 January 2019

Available online 29 January 2019

Keywords:

Nanotwins

Radiation

Detwinning

9R phase

Solute drag

ABSTRACT

Nanotwinned metals exhibit outstanding radiation tolerance as twin boundaries effectively engage, transport and eliminate radiation-induced defects. However, radiation-induced detwinning may reduce the radiation tolerance associated with twin boundaries, especially at elevated temperatures. Here we show, via *in-situ* Kr ion irradiation inside a transmission electron microscope, that 3 at. % Fe in epitaxial nanotwinned Cu (Cu₉₇Fe₃) significantly improves the thermal and radiation stability of nanotwins during radiation up to 5 displacements-per-atom at 200 °C. Such enhanced stability of nanotwins is attributed to a diffuse 9R phase resulted from the dissociation of incoherent twin boundaries in nanotwinned Cu₉₇Fe₃. The mechanisms for the enhanced stability of twin boundaries in irradiated nanotwinned alloys are discussed. The stabilization of nano-twins opens up opportunity for the application of nanotwinned alloys for aggressive radiation environments.

© 2019 Published by Elsevier Ltd on behalf of Acta Materialia Inc.

1. Introduction

Energetic particle irradiation of metallic materials produces large amounts of point defects (interstitials and vacancies), which can further aggregate into extended defect clusters in the form of dislocation loops [1–5], stacking fault tetrahedrons (SFTs) [6–11] or cavities [12–23], resulting in microstructural evolution and degradation of mechanical properties [24–29]. It has been proposed that the radiation tolerance of materials can be significantly improved by using defect sinks [30–35]. Nanostructured materials contain abundant defect sinks and have shown enhanced radiation tolerance [27,36–39]. Grain boundaries (GBs) are one of the effective defect sinks [40], and nanograined (NG) materials show enhanced radiation tolerance compared with their coarse-grained (CG) counterparts as evidenced by fewer defects [41,42], reduced radiation hardening [43], stronger resistance to amorphization [44] and much less void swelling [14,45]. However, due to the high

excess energy of conventional high-angle GBs, NG materials often suffer from poor thermal stability [46], and radiation-induced grain coarsening can occur even at room temperature [47]. Design of nanomaterials that can survive harsh radiation environments at elevated temperatures remains a major challenge [31,48].

Nanotwinned (NT) metals have raised significant interest due to their unique combination of remarkable mechanical properties [49–53] and superior thermal stability [54,55], as well as enhanced radiation tolerance [56–59]. *In-situ* studies have revealed that twin boundaries (TBs) can frequently interact with radiation-induced defects and tailor their formation and distribution [56,57,60–62]. For instance, fewer defects are formed in NT Cu than in CG Cu under the same radiation conditions [57]. In addition, SFT, a notorious defect, can be destructed by interacting with TBs [56].

In NT metals with face centered cubic (FCC) structure, there are two major types of TBs: $\Sigma 3$ {111} coherent twin boundaries (CTBs) and $\Sigma 3$ {112} incoherent twin boundaries (ITBs) [63,64]. Extensive studies have shown that ITBs, containing arrays of Shockley partials, can migrate under irradiation [65], stress [66], high temperature [67] and electrical field [68]. As a result, detwinning occurs

* Corresponding author.

E-mail address: xzhang98@purdue.edu (X. Zhang).

through ITB migration, decreases twin density, and compromises the performance of NT materials [69,70]. Therefore, to further improve the radiation tolerance of NT metals, it is of great significance to stabilize TBs, especially the highly mobile ITBs.

In this paper, we successfully synthesized epitaxial NT-Cu₉₇Fe₃ and compared its radiation response to that of NT-Cu by using *in-situ* Kr⁺⁺ irradiation at 200 °C inside a transmission electron microscope (TEM). The *in-situ* studies show that, in contrast to rapid detwinning in NT-Cu, the sharp ITBs in NT-Cu₉₇Fe₃ evolve into diffuse 9R phase and are highly stable against radiation at elevated temperatures. ITB migration velocity in NT-Cu₉₇Fe₃ is significantly lower than that in NT-Cu, lending experimental support for stabilizing NT structures via the introduction of certain solutes. *In-situ* studies also show that ITBs and CTBs in NT-Cu₉₇Fe₃ actively engage and eliminate radiation-induced defects.

2. Experimental methods

Highly-textured NT-Cu and NT-Cu₉₇Fe₃ alloy films, ~2 μm thick, were deposited on HF etched Si (110) substrates by using direct current magnetron sputtering technique at room temperature. Pure Cu (99.995%) and Fe (99.99%) targets were used for sputtering, and the chamber was evacuated to a base pressure ~5 × 10⁻⁸ torr prior to deposition. During deposition, ~1.2 × 10⁻³ torr Ar working pressure was used, and the deposition rate was controlled at ~0.6 nm/s. After depositions, the TEM specimens for irradiations were prepared by polishing, dimpling and low energy (3.5 keV) Ar ion milling. Subsequent heavy ion (1 MeV Kr⁺⁺) irradiations on the cross-sectional TEM samples were conducted in the Intermediate Voltage Electron Microscope (IVEM) at Argonne National Laboratory, where an ion accelerator was attached to a Hitachi-9000 TEM microscope. More specific information regarding such *in-situ* heavy ion irradiation technique has been described elsewhere [71]. Before irradiation, the TEM specimens were annealed at 200 °C inside the IVEM column for 30 min. Then it was followed by Kr⁺⁺ irradiations at 200 °C. During the irradiation, a CCD camera was utilized to capture videos at 15 frames/s.

The texture of as-deposited films was analyzed using an X-ray diffraction technique on a Panalytical Empyrean X'pert PRO MRD diffractometer with a Cu Kα₁ source. All the as-prepared and irradiated TEM samples were examined by a Thermo Fischer Scientific/FEI Talos 200X analytical TEM with Super-X EDS detectors. The Stopping and Range of Ions in Matter (SRIM) simulation with Kinch-Pease method was used to estimate the radiation damage in unit of displacements-per-atom (dpa) [72,73]. As the Fe content is low in NT-Cu₉₇Fe₃, the radiation damage profile was simulated based on pure Cu. SRIM simulations calculated for pure Cu (Supplementary Fig. S1) show that ~99% of Kr ions have penetrated through TEM foils, leaving most radiation damage behind. The average ion dose rate was ~2.5 × 10⁻³ dpa/s, and the maximum radiation damage was 5 dpa with a total fluence of 1 × 10¹⁵ ions/cm².

3. Results

Fig. 1 demonstrates the texture analysis of as-deposited Cu and Cu₉₇Fe₃ films. The conventional two-theta scans in Fig. 1(a) show that both films are highly {111} textured. The Phi scans in Fig. 1(b) show the diffraction peaks from both twin and matrix orientations with nearly identical intensity, indicating the formation of significant growth twin structures.

Fig. 2 compares the microstructural evolution of NT-Cu and Cu₉₇Fe₃. Cross-section TEM micrographs show that nanotwins in Cu have a smaller average twin spacing, ~5 nm, comparing with ~14 nm for the NT-Cu₉₇Fe₃. The twin spacing here is defined as the

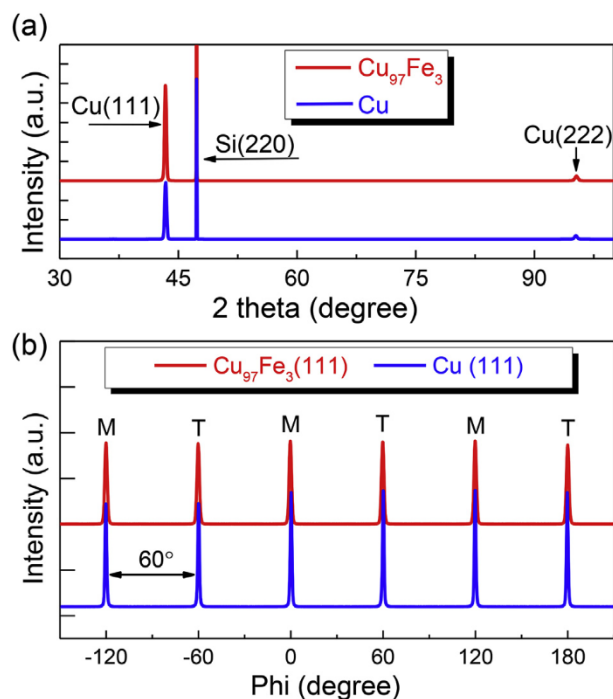


Fig. 1. (Color online) Texture analysis of XRD profiles of sputtered Cu (blue) and Cu₉₇Fe₃ films (red) on Si (110) substrates. (a) Two-theta scans showing strong (111) texture along growth direction for both films. (b) Phi-scan profiles with a six-fold symmetry, indicating a significant fraction of twins in both Cu and Cu₉₇Fe₃ films. M and T denote three matrix and twin peaks, respectively. (For interpretation of the references to colour in this figure legend, the reader is referred to the Web version of this article.)

distance between two adjacent CTBs [57]. No obvious TB migrations were observed during the annealing process at 200 °C for 30 min. However, once radiation started, detwinning took place in NT-Cu, giving rise to significant increase in twin spacing, as shown in Fig. 2(a1-a4). In contrast, nanotwins in NT-Cu₉₇Fe₃ exhibited superior stability, and most of TBs survived after irradiation to 5 dpa, as shown in Fig. 2(b1-b4). See supplementary video SV1 for more details. Statistical studies in Fig. 2(c1) and (c2) show the irradiation-induced prominent increase of average twin spacing (λ_{ave}) in NT-Cu from 5 to 29 nm (after 5 dpa), while the λ_{ave} in NT-Cu₉₇Fe₃ increased slightly from 14 to 16 nm.

Supplementary video related to this article can be found at <https://doi.org/10.1016/j.actamat.2019.01.037>.

The irradiation-induced detwinning event is attributed to defect-TB interactions. Fig. 3 compares the irradiation response of CTBs. It has been found that CTBs can become curved to accommodate defect clusters formed in the vicinity. Since defect clusters are often small and have transient lifetime [62,74], they introduce local and temporary distortion (in form of curvatures) along CTBs. As shown in Fig. 3, the local curved CTBs were frequently observed in both cases and they exhibited surprising resilience and self-healing ability. In NT-Cu at ~1.8 dpa in Fig. 3(a1), the CTBs appeared straight. After 6 s in Fig. 3(a2), the CTB became curved. However, by 19 s in Fig. 3(a3), the distorted CTB had recovered and restored its straight appearance. Similarly, in NT-Cu₉₇Fe₃, the upper CTB appeared straight initially (~2.5 dpa) in Fig. 3(b1). At 6 s in Fig. 3(b2), a local distortion was identified at position 1. By 25 s in Fig. 3(b3), the distortion 1 had recovered, while a new distortion at position 2 occurred due to the interaction between the CTB and a defect cluster. At 27 s in Fig. 3(b4), the distortion 2 also recovered. More detailed information can be found in supplementary videos of

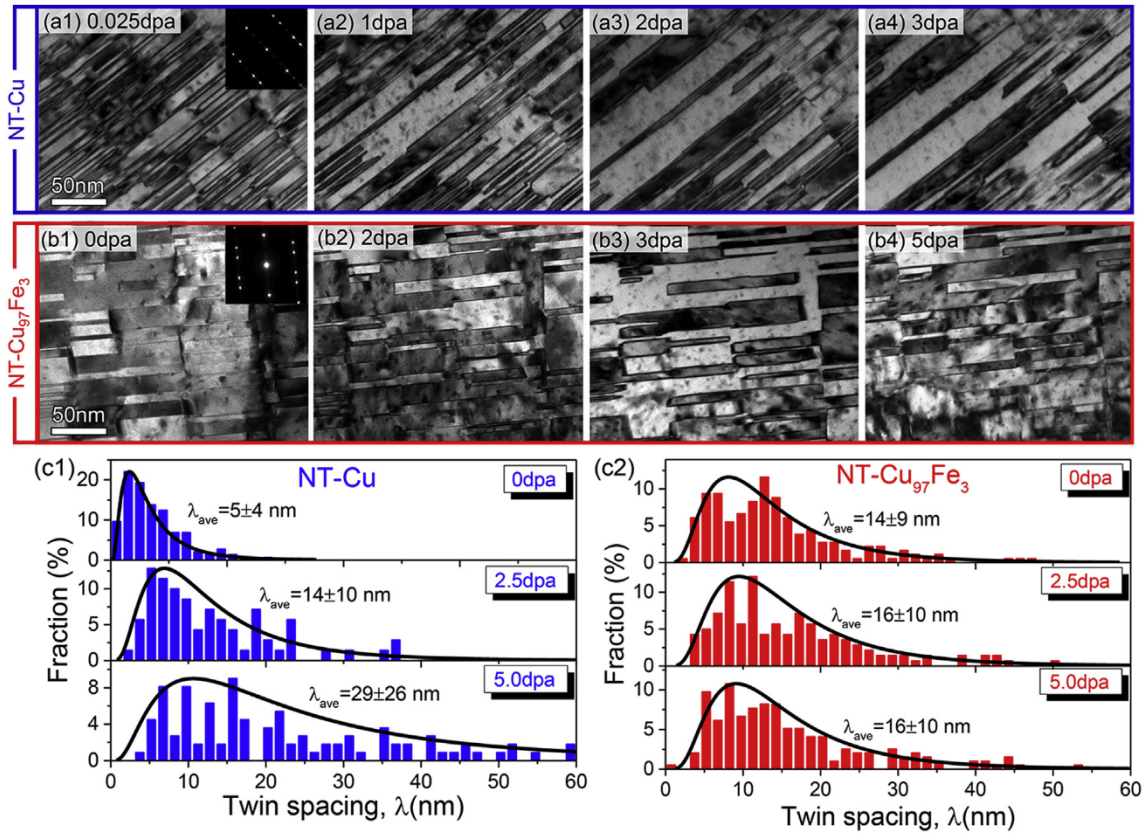


Fig. 2. Evolution of nanotwins in NT-Cu and NT-Cu₉₇Fe₃ under Kr⁺⁺ irradiation at 200 °C. (a1-a4) Irradiation-induced significant decrease of twin density in NT-Cu. (b1-b4) Superior stability of nanotwins against irradiation in NT-Cu₉₇Fe₃ to 5 dpa. (c1-c2) Statistical distributions show that the average twin spacing (λ_{ave}) of irradiated NT-Cu increases significantly from 5 to 29 nm, whereas the λ_{ave} in NT-Cu₉₇Fe₃ increases slightly from 14 to 16 nm. See supplementary video SV1 for more details.

SV2 and SV3.

Supplementary video related to this article can be found at <https://doi.org/10.1016/j.actamat.2019.01.037>.

By comparison, the ITBs in irradiated NT-Cu frequently migrated and showed prominent thickness-dependence. When the twin

thickness (t) is several nanometers, ITBs migrate drastically. As shown in Fig. 4(a), an ultrafine twin (3 nm in thickness) was 79 nm long at 0 s (~0.1 dpa). At 2 s in Fig. 4(b), its ITB migrated abruptly by 38 nm. By 10 s in Fig. 4(c), the twin had fully retracted (disappeared). More detailed information can be found in Supplementary Video SV4.

Supplementary video related to this article can be found at <https://doi.org/10.1016/j.actamat.2019.01.037>.

However, when $t > 10$ nm, ITB migration often starts from twin corners. As shown in Fig. 5(a1) at ~3.1 dpa, T1 ($t_1 = 13$ nm) had a

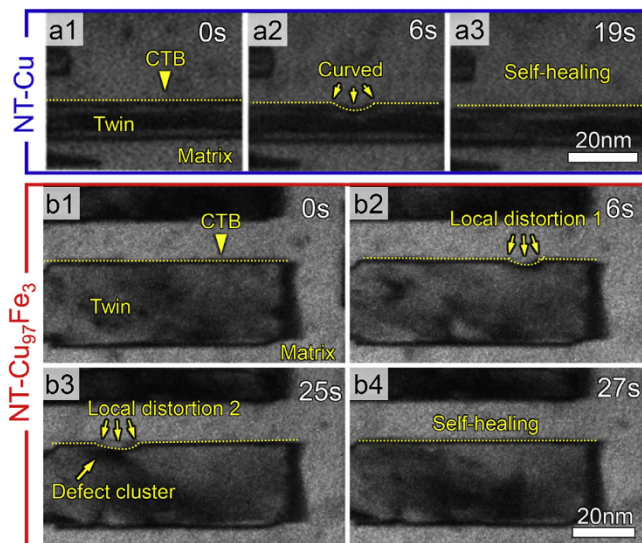


Fig. 3. Local distortion and self-healing capacity of CTBs in NT-Cu (a1-a3) and NT-Cu₉₇Fe₃ (b1-b4). See supplementary videos of SV2 and SV3 for more details.

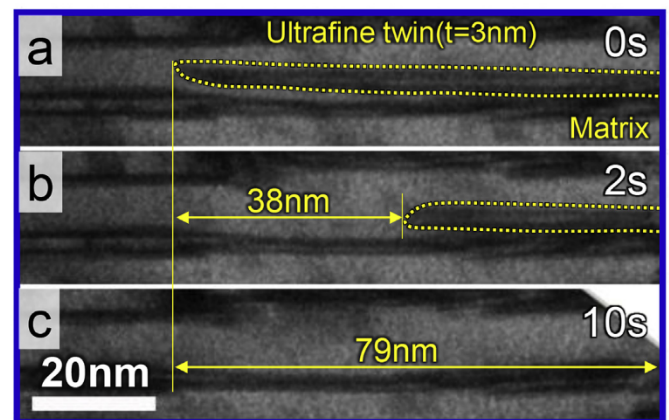


Fig. 4. The drastic ITB migration of an ultrafine twin (~3 nm in thickness) in NT-Cu. See supplementary video SV4.

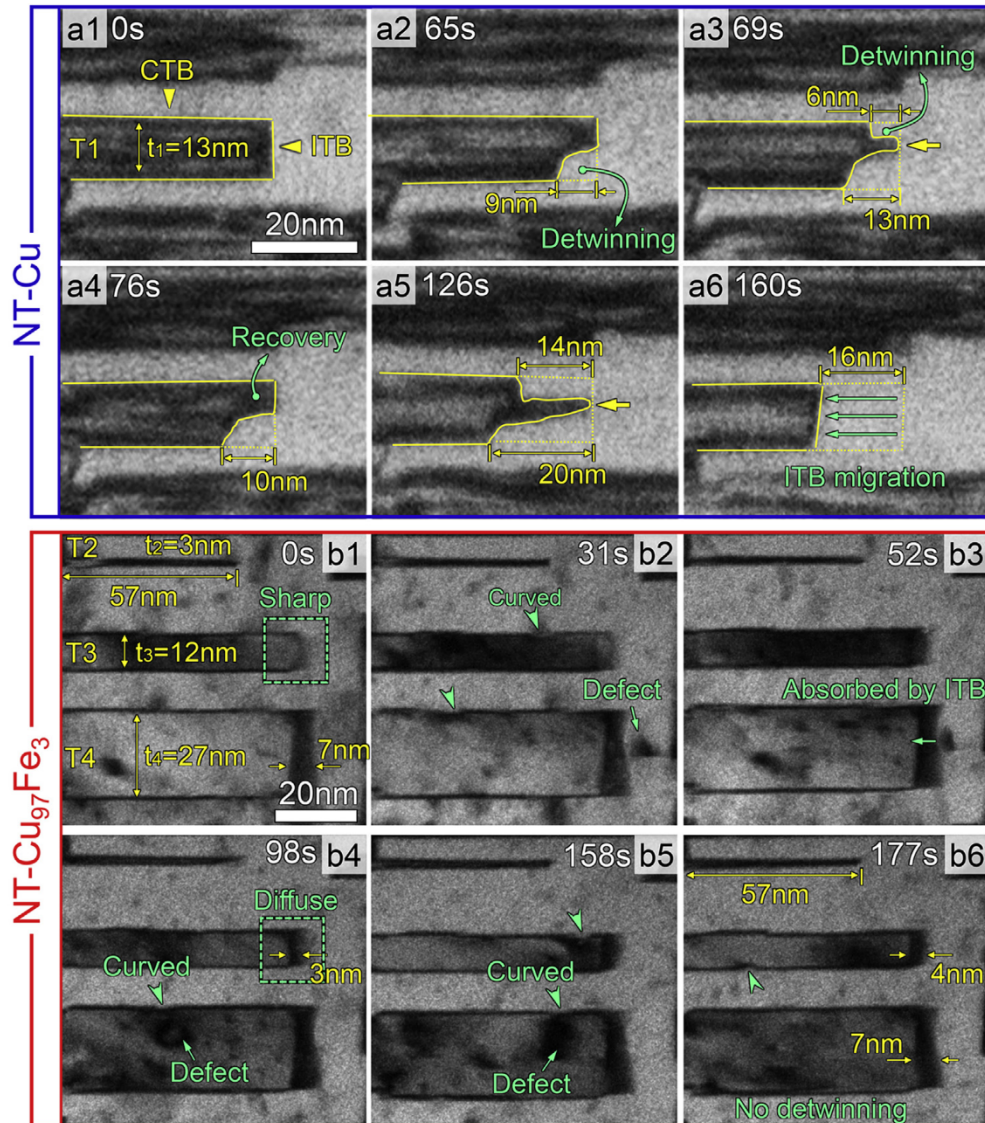


Fig. 5. *In-situ* TEM snapshots comparing the distinct irradiation responses of ITBs between NT-Cu and NT-Cu₉₇Fe₃. (a1–a6) The gradual ITB migration and detwinning of T1 ($t_1 = 13$ nm) in NT-Cu (3.1–3.5 dpa). (b1–b6) The stability of TBs against irradiation (2.4–2.8 dpa) in NT-Cu₉₇Fe₃. No detwinning was observed regardless of twin thickness. See supplementary videos SV5 and SV6 for more details.

vertical ITB with two right corners. In 65 s in Fig. 5(a2), the lower right corner retracted leftward by 10 nm and continued to retract by 13 nm after 69 s in Fig. 5(a3). Meanwhile, the upper corner experienced detwinning by 6 nm by 65 s, and recovery by 76 s as shown in Fig. 5(a4). With further irradiation to 126 s, both corners retracted by 14 nm and 20 nm, respectively, leading to a sharp tip in the middle of the ITB as shown in Fig. 5(a5). The protrusion remained unchanged, until significant detwinning occurred instantaneously at 160 s in Fig. 5(a6).

By comparison, the ITBs in NT-Cu₉₇Fe₃ remained stable regardless of twin thickness. For instance, three typical twins (T2, T3 and T4) with various thickness were monitored during irradiation (2.4–2.8 dpa) as shown in Fig. 5(b1–b6). No ITB migration was observed, even for the ultrafine twin T2 ($t_2 = 3$ nm). Note that the ITB of T3 ($t_3 = 12$ nm), as shown in the box in Fig. 5(b1), was initially sharp, but subsequently dissociated into a 3-nm-wide diffuse ITB after 98 s in Fig. 5(b4). The diffuse ITB extended further to be 4 nm wide, as shown in Fig. 5(b6). T4 ($t_4 = 27$ nm) has a diffuse ITB, which is 7 nm wide and its width remained unchanged

during irradiation. The diffuse ITB absorbed a large defect cluster, an SFT in its vicinity, as shown in Fig. 5(b2–b3). Meanwhile, CTBs also actively engaged in absorbing defects and became curved locally, as marked by the green arrows in Fig. 5(b2–b6). More details related to the irradiation responses of ITBs in NT-Cu and NT-Cu₉₇Fe₃ can be found in supplementary videos SV5 and SV6.

Supplementary video related to this article can be found at <https://doi.org/10.1016/j.actamat.2019.01.037>.

High-resolution TEM (HRTEM) experiments were performed to examine the evolution of TBs in irradiated NT-Cu and NT-Cu₉₇Fe₃ along $\langle 110 \rangle$ zone axis. Before irradiation, as shown in Fig. 6(a1) and (b1), the CTBs are sharp, and the ITB width is narrow, ~ 1 nm in both systems. After irradiation to 5 dpa, numerous stacking faults (SFs) emerged in NT-Cu along CTBs, and the thickness of SF ribbon is ~ 2 nm, whereas the thickness of CTBs in irradiated NT-Cu₉₇Fe₃ increases slightly in Fig. 6(b2). The ITBs of irradiated NT-Cu remain narrow (~ 1 nm), while the irradiated ITBs in NT-Cu₉₇Fe₃ have dissociated into a slab bounded by two curved phase boundaries. A typical example of the dissociated ITB in NT-Cu₉₇Fe₃ is shown in

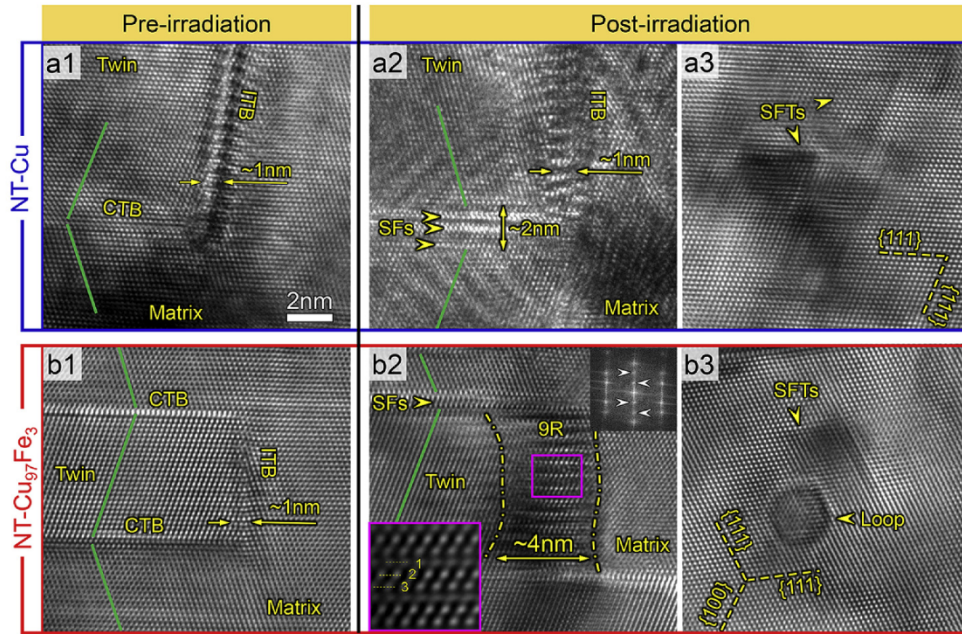


Fig. 6. HRTEM micrographs of TBs and irradiation-induced defects in NT-Cu and NT-Cu₉₇Fe₃ before and after irradiation (5 dpa). (a1) and (b1) TBs are sharp in both systems prior to irradiation. (a2) In irradiated NT-Cu, ITBs remain sharp, but CTBs are decorated with SF ribbons. (a3) Irradiation-induced triangular SFTs in NT-Cu. (b2) Radiation of NT-Cu₉₇Fe₃ induces broad ITBs, identified as 9R; but CTBs remain largely unchanged. (b3) The irradiated NT-Cu₉₇Fe₃ contains SFTs and prismatic dislocation loops.

Fig. 6(b2). The lower-left inset shows that the dissociated ITB region has a repeatable pattern, identified as 9R phase, which is also confirmed by the inserted fast Fourier transform (FFT). Note that in Fig. 5(b6) the dissociated ITB region of T4 is wider than that of T3, and it appears that the width of dissociated ITBs varies with twin thickness as will be shown later. HRTEM images in Fig. 6(a3) and (b3) also reveal that the defect clusters in NT-Cu are dominated by high-density triangular SFTs, whereas the defects in NT-Cu include SFTs and prismatic dislocation loops.

In-situ TEM technique permits the determination of ITB migration velocity (V_{ITB}). Fig. 7(a) indicates that irradiation induces ITB migration in NT-Cu, and the V_{ITB} decreases with increasing thickness (t). Moreover, V_{ITB} of NT-Cu increases significantly with increasing irradiation temperature (to 200 °C). In contrast, the ITBs in NT-Cu₉₇Fe₃ barely migrate during irradiation at 200 °C. In addition, Fig. 7(b) illustrates that the ITB width (W_{ITB}) of irradiated NT-

Cu has little variation and remains ~1 nm. In comparison, the W_{ITB} of irradiated NT-Cu₉₇Fe₃ elevates with increasing t , ranging from 3 to 10 nm.

4. Discussion

4.1. Thickness and temperature dependent detwinning in NT-Cu

Our *in-situ* TEM observations reveal that CTBs exhibit surprising resilience and self-healing ability in response to irradiation, as shown in Fig. 3. This is determined by the nature of irradiation-induced defect clusters and interactions with CTBs. Since defect clusters are often small and have transient lifetime [62,74], they introduce only local and temporary distortion (in form of curvatures) along CTBs. Moreover, previous studies show that the SFT-CTB interactions can lead to the formation of multiple SFs [56,74].

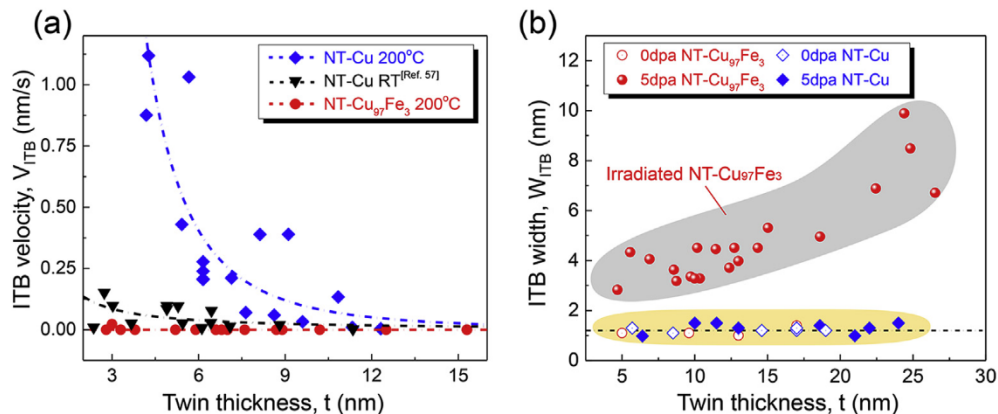


Fig. 7. (Color online) Irradiation-induced evolution of ITB velocity (V_{ITB}) and width (W_{ITB}), plotted as a function of twin thickness (t) for NT-Cu and NT-Cu₉₇Fe₃. (a) V_{ITB} increases rapidly with decreasing twin thickness for NT-Cu or at higher irradiation temperature. A reference black data set of NT-Cu irradiated at room temperature (RT) is also plotted [57]. The V_{ITB} is extremely low and barely changes for NT-Cu₉₇Fe₃ even for finest twins ($t < 5$ nm). (b) W_{ITB} of NT-Cu remains constant, ~1 nm, after radiation. However, the W_{ITB} of the irradiated NT-Cu₉₇Fe₃ increases monotonically with t . (For interpretation of the references to colour in this figure legend, the reader is referred to the Web version of this article.)

This is also confirmed by our post-irradiation HRTEM analysis in Fig. 6(a2) and Fig. 6(b2), which show that CTBs appear ‘thicker’ after irradiation.

Our *in-situ* observations also show that irradiation-induced detwinning occurs primarily through ITB migration. The ITBs in FCC Cu are composed of three types of mobile Shockley partials on

successive (111) planes [75–77]. Fig. 8(a1) schematically illustrates the ITB structure, including one pure edge partial (b_1) and two mixed partials (b_2 and b_3). This dislocation model has the advantage of relating ITB structure to its migration or dissociation.

ITBs in pure metals can migrate under shear stress through the collective glide of partials [78,79], known as the phase-boundary-

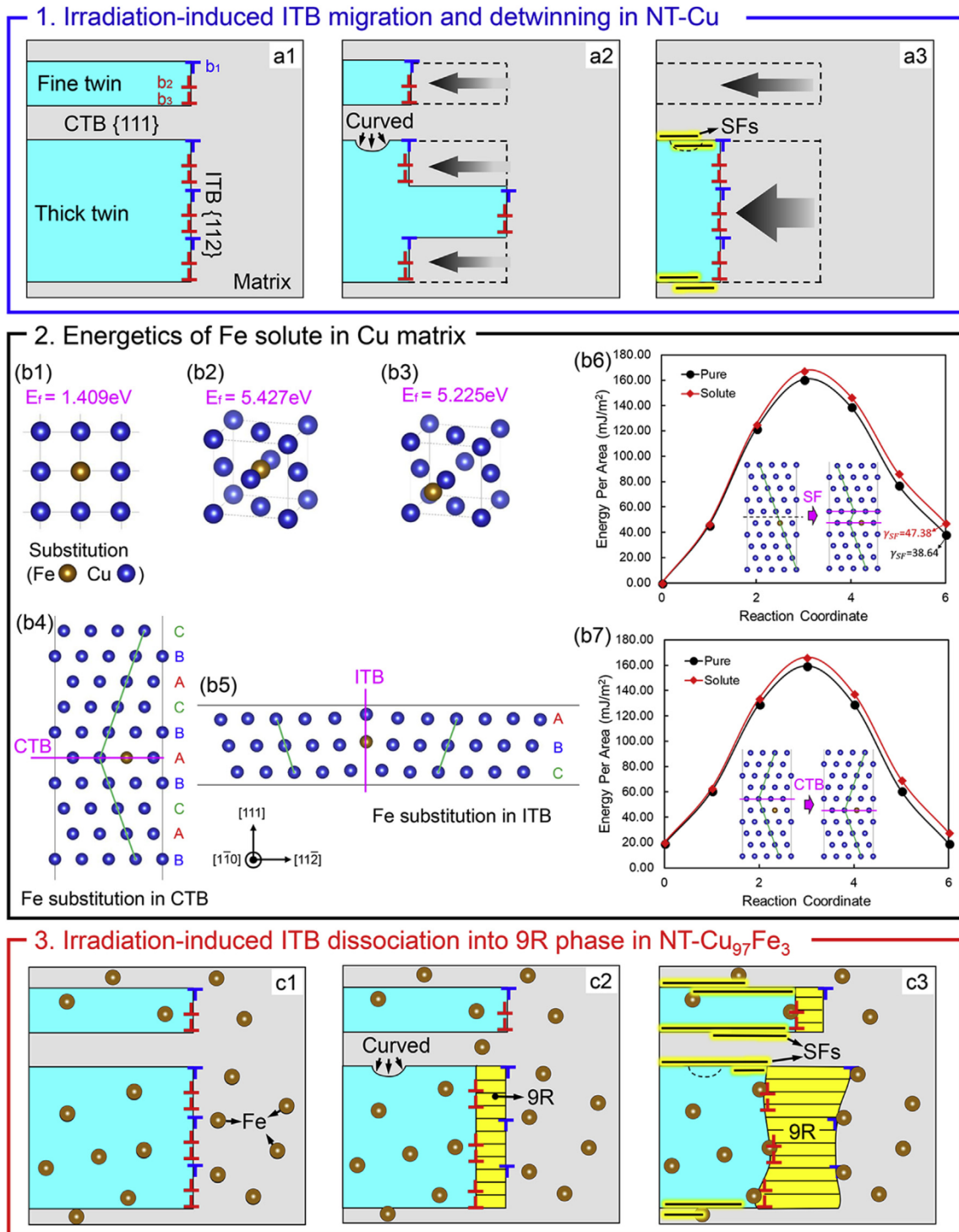


Fig. 8. (Color online) Irradiation responses of TBs in NT-Cu and NT-Cu₉₇Fe₃. (a1–a3) Irradiation-induced ITB migration and detwinning in NT-Cu. (b1–b7) DFT calculations of the energetics of Fe solute in Cu lattice, SF plane, CTB and ITB. (c1–c3) Irradiation of NT-Cu₉₇Fe₃ induces dissociation of ITBs into 9R phase, which is pinned by Fe solute atoms, and thus prohibit detwinning. In addition, irradiation can cause CTB distortions in form of curved TBs in both NT-Cu and NT-Cu₉₇Fe₃. (For interpretation of the references to colour in this figure legend, the reader is referred to the Web version of this article.)

migration (PBM) mechanism [80,81]. Impingement of defect clusters during radiation can enhance TB migration by lowering the activation energy barrier for dislocation glide [82]. Consequently, heavy ion irradiation induces ITB migration and detwinning in NT-Cu, as shown schematically in Fig. 8(a1–a3). The ITB migration velocity, V_{ITB} , in NT-Cu is closely associated with twin thickness (t). The driving force, $2\gamma_{Twin}/t$, for ITB migration increases with decreasing t [57], and γ_{Twin} is twin boundary energy for $\Sigma 3 \{111\}$, approximately $1/2$ of γ_{SF} , with γ_{SF} being the stacking fault energy (SFE). When t is comparable to the size of defect clusters, the entire ITB can migrate rapidly (see Fig. 4), and thus a fine twin is more likely to undergo detwinning, as shown in Fig. 8(a2–a3). For a thicker twin ($t > 10$ nm), however, detwinning often starts from twin corners, presumably because the migration of ITBs from corners does not change the total length or energy of the TBs [67]. If this analysis is correct, the reverse process, twinning from corner should also occur when local shear stress reverses its sign. Indeed, this hypothesis has been confirmed by our *in-situ* TEM observations in Fig. 5(a3–a4). At elevated temperatures, the Shockley partials possess higher mobility due to a reduced friction stress, and the driving force for detwinning also increases, and thus the ITB migration velocity increases further in NT-Cu.

4.2. Energetics of Fe solutes in Cu

In-situ studies show that a small amount of Fe solute atoms (~ 3 at. %) in NT-Cu can significantly enhance TBs stability against irradiation at elevated temperatures. First, there is much less detwinning in the irradiated NT-Cu₉₇Fe₃ alloy irrespective of original twin thickness (see Fig. 2). Many fine twins survived irradiation, in drastic contrast to the rapid detwinning in NT-Cu. Second, the TB migration velocity in NT-Cu increases sharply with decreasing twin thickness. In the irradiated NT-Cu₉₇Fe₃, however, TBs barely migrate. Third, our study shows that ITB migration velocity in NT-Cu increases significantly during irradiation at elevated temperatures. Irradiation of NT-Cu₉₇Fe₃ at the same temperature leads to little sign of detwinning.

To understand the influence of Fe on TB stability, we examined the energetics of Fe solute in Cu lattice with respect to their locations according to density functional theory (DFT) calculations. The detailed calculation procedure can be found in the Supplementary Information. The results show that the formation energy (E_f) of a single Fe solute is 1.409 eV for substitutional site (Fig. 8(b1)), 5.427 eV for tetrahedral interstitial (Fig. 8(b2)) and 5.225 eV for octahedral interstitial site (Fig. 8(b3)). In comparison, E_f of Cu self-interstitial atom for tetrahedral and octahedral site is 3.901 and 3.488 eV, respectively, much lower than that of Fe interstitial. These results show that Fe solute prefers to stay at substitutional site and can hardly diffuse via interstices. E_f of Fe substitutional pair located at different neighboring sites is also calculated. For the first, second, third, and fourth nearest sites, the formation energies are 2.294, 2.744, 2.805 and 2.766 eV, respectively. E_f of four Fe atoms at nearest substitutional sites is 1.533 eV. Therefore, the segregation of Fe atoms is energetically preferred. But, as mentioned earlier, the diffusion of Fe is energetically difficult, so the Fe solutes are expected to be homogeneously distributed in Cu matrix during deposition, which is consistent with our EDS analysis shown in Supplementary Fig. S2.

The formation energies of Fe solutes at SF plane, CTB (Fig. 8(b4)) and ITB (Fig. 8(b5)) are also calculated. As shown in Fig. 8(b6), the calculated stacking fault energy (γ_{SF}) of pure Cu is 38.64 mJ/m². If one of the 16 Cu atoms on a fault plane is replaced by an Fe atom, the stacking fault energy increases to 47.38 mJ/m². For the model with CTB, the segregation energy of Fe, the energy change for moving Fe atom from defect free crystal to the twin boundary, is

0.048 eV, which suggests that the CTB is not the preferred site for Fe solutes. The energy barrier of CTB migration shown in Fig. 8(b7) increases by adding Fe solutes. In addition, the formation energies of Fe solutes in ITB at substitutional and interstitial sites are 0.623–0.824 eV and 1.669–1.750 eV, respectively. The lower formation energies indicate that ITBs are thermodynamically favorable sites for Fe solutes.

4.3. Mechanisms of irradiation stability of nanotwins in NT-Cu₉₇Fe₃

Post-radiation TEM studies in Fig. 6(b2) show that the ITBs in irradiated NT-Cu₉₇Fe₃ dissociate into a broad 9R phase, bounded by two phase boundaries. Furthermore, the width of 9R phase increases with increasing twin thickness, as illustrated in Fig. 7(b). Such an observation has profound impact on TB stability and radiation tolerance of irradiated NT Cu–Fe alloys and warrants further discussions.

First, the ITB dissociation occurs through the glide of arrays of Shockley partials [77,83]. When an ITB is subjected to shear, τ_{yx} , the glide force on the partial dislocation b_1 is expressed by Ref. [81]:

$$F_x = -\tau_{yx}b_1 + F_{b_1b_2} + F_{b_1b_3} + \gamma_{SF} + F_p \quad (1)$$

The first term on the right in Equation (1) represents the driving force for migration of b_1 under external shear stress. The resistance for the migration of b_1 arises from $F_{b_1b_2}$ and $F_{b_1b_3}$, the attractive force between b_1 and b_2 (b_3); the stacking fault energy, γ_{SF} , and the friction force due to Peierls stress, F_p . During irradiation of monolithic NT-Cu, defect clusters will generate a shear stress that drives the migration of ITBs [60]. The γ_{SF} of Cu is low, and F_p is typically negligible in Cu, and thus the resistance to the migration of TB is relatively low.

Our DFT calculations show that Fe can increase the γ_{SF} , consequently the resistance for ITB migration increases substantially in NT Cu₉₇Fe₃ alloys. Also the growth twin density in as-deposited NT-Cu₉₇Fe₃ is lower than that in as-deposited NT-Cu, in agreement with the twin nucleation theory in sputtered films that suggests a higher γ_{SF} leads to a lower probability of twin nucleation [51]. Moreover, post-radiation TEM studies show that a majority of defect clusters in irradiated NT-Cu are SFTs; however, both SFTs and large prismatic dislocation loops are observed in irradiated NT-Cu₉₇Fe₃ alloy. Prismatic loops are often observed in irradiated materials with higher γ_{SF} [84].

Second, it has been shown in monolithic NT metals, that the edge Shockley partial and two mixed partials migrate together due to their mutual attractive forces [81]. MD simulations have shown that the edge partial, b_1 , tends to migrate first under shear. The attractive force between b_1 and b_2 (b_3) then drags the two mixed partials to move together, leading to the migration of ITBs. The current study shows that radiation of NT-Cu did not change the width of ITBs, ~ 1 nm. However, the width of ITBs in irradiated NT-Cu₉₇Fe₃ increases rapidly during irradiation to 3–10 nm. Thus, the attractive force between b_1 and b_2 (b_3) decreases, making the migration of ITBs difficult. Previous *in-situ* TEM studies showed that broad 9R in twinned Ag is unstable, and can “zip” together into a sharp ITB under e-beam irradiation to relax internal stress, and migrates rapidly thereafter [83]. As the 9R phase is stabilized by Fe solute and remains broad in the irradiated NT-Cu₉₇Fe₃, its migration becomes difficult.

Third, our *in-situ* radiation studies in Fig. 5(b1–b6) show that 9R phase in NT Cu₉₇Fe₃ is an excellent defect sink, as it can capture and absorb defect clusters, such as dislocation loops and SFTs. Consequently, the 9R phase becomes broader, as schematically shown in Fig. 8(c2). Since thicker twins have greater probability to capture defect clusters [74], the width of their 9R increases with twin

thickness, as shown in Fig. 8(c3). 9R and CTBs can thus form an effective defect-sink network, contributing to the remarkable radiation tolerance of NT-Cu₉₇Fe₃ alloy.

The dissociation of an ITB into 9R phase has been reported in pure Au [85], Ag [86] and Cu [76] with low γ_{SF} [87]. It has been concluded that the degree to which ITBs dissociate depends not only on the local stress state within specimen but also on the stacking fault energy [88]. Our study suggests that using appropriate solutes may effectively stabilize 9R phase in various metallic materials. Recently, high-density 9R phase has also been reported in sputtered NT Al-Fe [89], Al-Ti [90] and Al-Mg [91] solid solution alloys. These studies reveal that 9R phase is also beneficial for improving the mechanical properties (high strength and plasticity) of NT metals. The current study suggests that 9R phase coupled with the selection of appropriate solutes may significantly enhance the radiation resistance and stability of nanotwins in a broad range of metallic materials.

5. Conclusions

Nanotwinned Cu and Cu₉₇Fe₃ were *in-situ* irradiated using Kr⁺⁺ at 200 °C under the same condition inside a transmission electron microscope. Monolithic NT-Cu experiences prominent detwinning through ITB migration, whereas the nanotwins in NT-Cu₉₇Fe₃ alloy remain stable. The outstanding radiation and thermal stability of TBs in NT-Cu₉₇Fe₃ arise from the dissociation of ITBs into a broad 9R phase, which also actively absorbs radiation-induced defects. The enhanced twin stability is also attributed to the drag effect of Fe solutes on the dissociated ITBs. These findings provide an important step forward towards the design of stable radiation-resistant nanotwinned alloys under extreme environments.

Acknowledgements

We acknowledge primary financial support by NSF-CMMI-MOM Program under grant no. 1728419. The work on fabrication of nanotwinned metals is supported by DOE-BES under grant no. DE-SC0016337. We also thank Peter M. Baldo and Edward A. Ryan at Argonne National Laboratory for their help during *in-situ* radiation experiments. The IVEM facility at Argonne National Laboratory is supported by DOE-Office of Nuclear Energy. Accesses to the Microscopy Centers at Purdue University and the DOE Center for Integrated Nanotechnologies managed by Los Alamos National Laboratory is also acknowledged. D.Y. Xie and J. Wang acknowledge the support by the Nebraska Center for Energy Sciences Research, University of Nebraska-Lincoln, University of Nebraska-Lincoln. Atomistic simulations were completed utilizing the Holland Computing Center of the University of Nebraska, which receives support from the Nebraska Research Initiative. We also acknowledge the support by Center for Nanoscale Materials (CNM) at Argonne National Laboratory under CNM Proposal 52081.

Appendix A. Supplementary data

Supplementary data to this article can be found online at <https://doi.org/10.1016/j.actamat.2019.01.037>.

References

- [1] J. Silcox, P. Hirsch, Dislocation loops in neutron-irradiated copper, *Phil. Mag.* 4 (48) (1959) 1356–1374.
- [2] S. Zinkle, R. Sindelar, Defect microstructures in neutron-irradiated copper and stainless steel, *J. Nucl. Mater.* 155 (1988) 1196–1200.
- [3] B.D. Wirth, How does radiation damage materials? *Science* 318 (5852) (2007) 923–924.
- [4] C.J. Ulmer, A.T. Motta, M.A. Kirk, *In situ* ion irradiation of zirconium carbide, *J. Nucl. Mater.* 466 (2015) 606–614.
- [5] M. Jenkins, Characterisation of radiation-damage microstructures by TEM, *J. Nucl. Mater.* 216 (1994) 124–156.
- [6] S. Zinkle, G. Kulcinski, R. Knoll, Microstructure of copper following high dose 14-MeV Cu ion irradiation, *J. Nucl. Mater.* 138 (1) (1986) 46–56.
- [7] M. Jenkins, A weak-beam electron microscopy analysis of defect clusters in heavy-ion irradiated silver and copper, *Phil. Mag.* 29 (4) (1974) 813–828.
- [8] W. Sigle, M. Jenkins, J. Hutchison, Determination of the nature of stacking-fault tetrahedra in electron-irradiated silver by high-resolution structural imaging, *Phil. Mag. Lett.* 57 (5) (1988) 267–271.
- [9] S. Kojima, Y. Satoh, H. Taoka, I. Ishida, T. Yoshiie, M. Kiritani, Confirmation of vacancy-type stacking fault tetrahedra in quenched, deformed and irradiated face-centred cubic metals, *Philos. Mag.* A 59 (3) (1989) 519–532.
- [10] C. Lu, K. Jin, L.K. Béland, F. Zhang, T. Yang, L. Qiao, Y. Zhang, H. Bei, H.M. Christen, R.E. Stoller, Direct observation of defect range and evolution in ion-irradiated single crystalline Ni and Ni binary alloys, *Sci. Rep.* 6 (2016).
- [11] J. Li, C. Fan, J. Ding, S. Xue, Y. Chen, Q. Li, H. Wang, X. Zhang, *In situ* heavy ion irradiation studies of nanopore shrinkage and enhanced radiation tolerance of nanoporous Au, *Sci. Rep.* 7 (2017).
- [12] S.J. Zinkle, K. Farrell, Void swelling and defect cluster formation in reactor-irradiated copper, *J. Nucl. Mater.* 168 (3) (1989) 262–267.
- [13] B. Singh, On the influence of grain boundaries on void growth, *Phil. Mag.* 28 (6) (1973) 1409–1413.
- [14] M. Song, Y. Wu, D. Chen, X. Wang, C. Sun, K. Yu, Y. Chen, L. Shao, Y. Yang, K. Hartwig, Response of equal channel angular extrusion processed ultrafine-grained T91 steel subjected to high temperature heavy ion irradiation, *Acta Mater.* 74 (2014) 285–295.
- [15] C. Sun, S. Zheng, C. Wei, Y. Wu, L. Shao, Y. Yang, K. Hartwig, S. Maloy, S. Zinkle, T. Allen, Superior radiation-resistant nanoengineered austenitic 304L stainless steel for applications in extreme radiation environments, *Sci. Rep.* 5 (2015) 7801.
- [16] B. Muntifer, S.J. Blair, C. Gong, A. Dunn, R. Dingreville, J. Qu, K. Hattar, Cavity evolution at grain boundaries as a function of radiation damage and thermal conditions in nanocrystalline nickel, *Materials Research Letters* 4 (2) (2016) 96–103.
- [17] J. Li, C. Fan, Q. Li, H. Wang, X. Zhang, *In situ* studies on irradiation resistance of nanoporous Au through temperature-jump tests, *Acta Mater.* 143 (2017) 30–42.
- [18] D. Chen, N. Li, D. Yuryev, J.K. Baldwin, Y. Wang, M.J. Demkowicz, Self-organization of helium precipitates into elongated channels within metal nanolayers, *Science Advances* 3 (11) (2017).
- [19] C. Cawthorne, E. Fulton, Voids in irradiated stainless steel, *Nature* 216 (5115) (1967) 575–576.
- [20] C. Chen, The shapes of irradiation-produced voids in nickel, *Phys. Status Solidi* 16 (1) (1973) 197–210.
- [21] D. Chen, N. Li, D. Yuryev, J.K. Baldwin, Y. Wang, M.J. Demkowicz, Self-organization of helium precipitates into elongated channels within metal nanolayers, *Science Advances* 3 (11) (2017) eaao2710.
- [22] W. Xu, Y. Zhang, G. Cheng, W. Jian, P.C. Millett, C.C. Koch, S.N. Mathaudhu, Y. Zhu, *In-situ* atomic-scale observation of irradiation-induced void formation, *Nat. Commun.* 4 (2013) 2288.
- [23] C. Du, S. Jin, Y. Fang, J. Li, S. Hu, T. Yang, Y. Zhang, J. Huang, G. Sha, Y. Wang, Ultrastrong nanocrystalline steel with exceptional thermal stability and radiation tolerance, *Nat. Commun.* 9 (1) (2018) 5389.
- [24] S. Zinkle, 1.03-Radiation-Induced Effects on Microstructure, *Comprehensive Nuclear Materials*, Elsevier, Oxford, 2012, pp. 65–98.
- [25] G.S. Was, *Fundamentals of Radiation Materials Science: Metals and Alloys*, Springer, 2016.
- [26] Z. Shang, J. Li, C. Fan, Y. Chen, Q. Li, H. Wang, T. Shen, X. Zhang, *In situ* study on surface roughening in radiation-resistant Ag nanowires, *Nanotechnology* 29 (21) (2018) 215708.
- [27] X. Zhang, K. Hattar, Y. Chen, L. Shao, J. Li, C. Sun, K. Yu, N. Li, M.L. Taheri, H. Wang, Radiation damage in nanostructured materials, *Prog. Mater. Sci.* 96 (2018) 217–321.
- [28] S. Zinkle, G. Kulcinski, L. Mansur, Radiation-enhanced recrystallization in copper alloys, *J. Nucl. Mater.* 141 (1986) 188–192.
- [29] X. Zhang, K. Hattar, Y. Chen, L. Shao, J. Li, C. Sun, K. Yu, N. Li, M.L. Taheri, H. Wang, Radiation damage in nanostructured materials, *Prog. Mater. Sci.* 96 (2018) 217–321.
- [30] G. Ackland, Controlling radiation damage, *Science* 327 (5973) (2010) 1587–1588.
- [31] I. Beyerlein, A. Caro, M. Demkowicz, N. Mara, A. Misra, B. Uberuaga, Radiation damage tolerant nanomaterials, *Mater. Today* 16 (11) (2013) 443–449.
- [32] M. Demkowicz, R. Hoagland, J. Hirth, Interface structure and radiation damage resistance in Cu-Nb multilayer nanocomposites, *Phys. Rev. Lett.* 100 (13) (2008) 136102.
- [33] A. Misra, M. Demkowicz, X. Zhang, R. Hoagland, The radiation damage tolerance of ultra-high strength nanolayered composites, *JOM (J. Occup. Med.)* 59 (9) (2007) 62–65.
- [34] M. Demkowicz, P. Bellon, B. Wirth, Atomic-scale design of radiation-tolerant nanocomposites, *MRS Bull.* 35 (12) (2010) 992–998.
- [35] Y. Chen, K.Y. Yu, Y. Liu, S. Shao, H. Wang, M. Kirk, J. Wang, X. Zhang, Damage-tolerant nanotwinned metals with nanovoids under radiation environments, *Nat. Commun.* 6 (2015).
- [36] N. Li, M. Demkowicz, N. Mara, Y. Wang, A. Misra, Hardening due to interfacial

- He bubbles in nanolayered composites, *Materials Research Letters* 4 (2) (2016) 75–82.
- [37] A. Vattré, T. Jourdan, H. Ding, M.C. Marinica, M.J. Demkowicz, Non-random walk diffusion enhances the sink strength of semicoherent interfaces, *Nat. Commun.* 7 (2016) 10424.
- [38] M.J. Demkowicz, R.G. Hoagland, J.P. Hirth, Interface structure and radiation damage resistance in Cu-Nb multilayer nanocomposites, *Phys. Rev. Lett.* 100 (13) (2008) 136102.
- [39] K. Yu, Y. Chen, J. Li, Y. Liu, H. Wang, M.A. Kirk, M. Li, X. Zhang, Measurement of heavy ion irradiation induced in-plane strain in patterned face-centered-cubic metal films: an in situ study, *Nano Lett.* 16 (12) (2016) 7481–7489.
- [40] X.-M. Bai, A.F. Voter, R.G. Hoagland, M. Nastasi, B.P. Uberuaga, Efficient annealing of radiation damage near grain boundaries via interstitial emission, *Science* 327 (5973) (2010) 1631–1634.
- [41] M. Rose, A. Balogh, H. Hahn, Instability of irradiation induced defects in nanostructured materials, *Nucl. Instrum. Methods Phys. Res. Sect. B Beam Interact. Mater. Atoms* 127 (1997) 119–122.
- [42] K. Yu, Y. Liu, C. Sun, H. Wang, L. Shao, E. Fu, X. Zhang, Radiation damage in helium ion irradiated nanocrystalline Fe, *J. Nucl. Mater.* 425 (1) (2012) 140–146.
- [43] G. Cheng, W. Xu, Y. Wang, A. Misra, Y. Zhu, Grain size effect on radiation tolerance of nanocrystalline Mo, *Scripta Mater.* 123 (2016) 90–94.
- [44] T.D. Shen, S. Feng, M. Tang, J.A. Valdez, Y. Wang, K.E. Sickafus, Enhanced radiation tolerance in nanocrystalline Mg Ga₂O₄, *Appl. Phys. Lett.* 90 (26) (2007) 263115.
- [45] O. El-Atwani, J. Hinks, G. Greaves, J.P. Allain, S.A. Maloy, Grain size threshold for enhanced irradiation resistance in nanocrystalline and ultrafine tungsten, *Materials Research Letters* (2017) 1–7.
- [46] K. Lu, Stabilizing nanostructures in metals using grain and twin boundary architectures, *Nature Reviews Materials* 1 (2016) 16019.
- [47] D. Kaoumi, A. Motta, R. Birtcher, A thermal spike model of grain growth under irradiation, *J. Appl. Phys.* 104 (7) (2008) 073525.
- [48] S.J. Zinkle, G. Was, Materials challenges in nuclear energy, *Acta Mater.* 61 (3) (2013) 735–758.
- [49] L. Lu, Y. Shen, X. Chen, L. Qian, K. Lu, Ultrahigh strength and high electrical conductivity in copper, *Science* 304 (5669) (2004) 422–426.
- [50] D. Bufford, H. Wang, X. Zhang, High strength, epitaxial nanotwinned Ag films, *Acta Mater.* 59 (1) (2011) 93–101.
- [51] X. Zhang, A. Misra, H. Wang, T. Shen, M. Nastasi, T. Mitchell, J. Hirth, R. Hoagland, J. Embury, Enhanced hardening in Cu/330 stainless steel multilayers by nanoscale twinning, *Acta Mater.* 52 (4) (2004) 995–1002.
- [52] X. Zhang, H. Wang, X. Chen, L. Lu, K. Lu, R. Hoagland, A. Misra, High-strength sputter-deposited Cu foils with preferred orientation of nanoscale growth twins, *Appl. Phys. Lett.* 88 (17) (2006) 173116.
- [53] J. Wang, X. Zhang, Twinning effects on strength and plasticity of metallic materials, *MRS Bull.* 41 (04) (2016) 274–281.
- [54] O. Anderoglu, A. Misra, H. Wang, X. Zhang, Thermal stability of sputtered Cu films with nanoscale growth twins, *J. Appl. Phys.* 103 (9) (2008) 094322.
- [55] X. Zhang, A. Misra, Superior thermal stability of coherent twin boundaries in nanotwinned metals, *Scripta Mater.* 66 (11) (2012) 860–865.
- [56] K. Yu, D. Bufford, C. Sun, Y. Liu, H. Wang, M. Kirk, M. Li, X. Zhang, Removal of stacking-fault tetrahedra by twin boundaries in nanotwinned metals, *Nat. Commun.* 4 (2013) 1377.
- [57] Y. Chen, H. Wang, M. Kirk, M. Li, J. Wang, X. Zhang, Radiation induced detwinning in nanotwinned Cu, *Scripta Mater.* 130 (2017) 37–41.
- [58] C. Fan, Y. Chen, J. Li, J. Ding, H. Wang, X. Zhang, Defect evolution in heavy ion irradiated nanotwinned Cu with nanovoids, *J. Nucl. Mater.* 496 (2017) 293–300.
- [59] J. Li, D. Xie, S. Xue, C. Fan, Y. Chen, H. Wang, J. Wang, X. Zhang, Superior twin stability and radiation resistance of nanotwinned Ag solid solution alloy, *Acta Mater.* 151 (2018) 395–405.
- [60] J. Li, K. Yu, Y. Chen, M. Song, H. Wang, M. Kirk, M. Li, X. Zhang, In situ study of defect migration kinetics and self-healing of twin boundaries in heavy ion irradiated nanotwinned metals, *Nano Lett.* 15 (5) (2015) 2922–2927.
- [61] J. Li, Y. Chen, H. Wang, X. Zhang, In situ studies on twin-thickness-dependent distribution of defect clusters in heavy ion-irradiated nanotwinned Ag, *Metall. Mater. Trans.* 48 (3) (2017) 1466–1473.
- [62] C. Fan, J. Li, Z. Fan, H. Wang, X. Zhang, In situ studies on the irradiation-induced twin boundary-defect interactions in Cu, *Metall. Mater. Trans.* (2017) 1–9.
- [63] D.C. Bufford, Y.M. Wang, Y. Liu, L. Lu, Synthesis and microstructure of electrodeposited and sputtered nanotwinned face-centered-cubic metals, *MRS Bull.* 41 (4) (2016) 286–291.
- [64] I.J. Beyerlein, X. Zhang, A. Misra, Growth twins and deformation twins in metals, *Annu. Rev. Mater. Res.* 44 (2014) 329–363.
- [65] J. Du, Z. Wu, E. Fu, Y. Liang, X. Wang, P. Wang, K. Yu, X. Ding, M. Li, M. Kirk, Detwinning through migration of twin boundaries in nanotwinned Cu films under in situ ion irradiation, *Sci. Technol. Adv. Mater.* (2018) 1–23 (just-accepted).
- [66] Y. Liu, J. Jian, Y. Chen, H. Wang, X. Zhang, Plasticity and ultra-low stress induced twin boundary migration in nanotwinned Cu by in situ nano-indentation studies, *Appl. Phys. Lett.* 104 (23) (2014) 231910.
- [67] J. Miao, Structure and migration of (112) step on (111) twin boundaries in nanocrystalline copper, *J. Appl. Phys.* 104 (2008) 113717.
- [68] K.-C. Chen, W.-W. Wu, C.-N. Liao, L.-J. Chen, K. Tu, Stability of nanoscale twins in copper under electric current stressing, *J. Appl. Phys.* 108 (6) (2010), 066103.
- [69] K.Y. Yu, D. Bufford, F. Khatkhatay, H. Wang, M.A. Kirk, X. Zhang, In situ studies of irradiation induced twin boundary migration in nanotwinned Ag, *Scripta Mater.* 69 (2013) 385.
- [70] N. Li, J. Wang, Y. Wang, Y. Serruys, M. Nastasi, A. Misra, Incoherent twin boundary migration induced by ion irradiation in Cu, *J. Appl. Phys.* 113 (2) (2013), 023508.
- [71] M. Li, M. Kirk, P. Baldo, D. Xu, B. Wirth, Study of defect evolution by TEM with in situ ion irradiation and coordinated modeling, *Phil. Mag.* 92 (16) (2012) 2048–2078.
- [72] J.F. Ziegler, M.D. Ziegler, J.P. Biersack, SRIM—The stopping and range of ions in matter, *Nucl. Instrum. Methods Phys. Res. Sect. B Beam Interact. Mater. Atoms* 268 (11) (2010) 1818–1823, 2010.
- [73] R.E. Stoller, M.B. Toloczko, G.S. Was, A.G. Certain, S. Dwaraknath, F.A. Garner, On the use of SRIM for computing radiation damage exposure, *Nucl. Instrum. Methods Phys. Res. Sect. B Beam Interact. Mater. Atoms* 310 (2013) 75–80.
- [74] Y. Chen, J. Li, K. Yu, H. Wang, M. Kirk, M. Li, X. Zhang, In situ studies on radiation tolerance of nanotwinned Cu, *Acta Mater.* 111 (2016) 148–156.
- [75] G.H. Campbell, D.K. Chan, D.L. Medlin, J.E. Angelo, C.B. Carter, Dynamic observation of the fcc to 9R shear transformation in a copper $\Sigma = 3$ incoherent twin boundary, *Scripta Mater.* 35 (7) (1996) 837–842.
- [76] C.B. Carter, D. Medlin, J. Angelo, M.J. Mills, The 112 Lateral Twin Boundary in FCC Metals, *Materials Science Forum*, Trans Tech Publ, 1996, pp. 209–212.
- [77] J. Wang, O. Anderoglu, J. Hirth, A. Misra, X. Zhang, Dislocation structures of $\Sigma 3$ {112} twin boundaries in face centered cubic metals, *Appl. Phys. Lett.* 95 (2) (2009), 021908.
- [78] N. Li, J. Wang, J. Huang, A. Misra, X. Zhang, Influence of slip transmission on the migration of incoherent twin boundaries in epitaxial nanotwinned Cu, *Scripta Mater.* 64 (2) (2011) 149–152.
- [79] N. Li, J. Wang, X. Zhang, A. Misra, In-situ TEM study of dislocation-twin boundaries interaction in nanotwinned Cu films, *J. Occup. Med.* 63 (9) (2011) 62–66.
- [80] J. Wang, A. Misra, J. Hirth, Shear response of $\Sigma 3$ {112} twin boundaries in face-centered-cubic metals, *Phys. Rev. B* 83 (6) (2011), 064106.
- [81] J. Wang, N. Li, O. Anderoglu, X. Zhang, A. Misra, J. Huang, J. Hirth, Detwinning mechanisms for growth twins in face-centered cubic metals, *Acta Mater.* 58 (6) (2010) 2262–2270.
- [82] D. Song, X. Li, J. Xue, H. Duan, Z. Jin, Irradiation-enhanced twin boundary migration in BCC Fe, *Phil. Mag. Lett.* 94 (6) (2014) 361–369.
- [83] L. Liu, J. Wang, S. Gong, S. Mao, High resolution transmission electron microscope observation of zero-strain deformation twinning mechanisms in Ag, *Phys. Rev. Lett.* 106 (17) (2011) 175504.
- [84] S. Zinkle, L. Seitzman, W. Wolfer, I. Energy calculations for pure metals, *Philos. Mag.* A 55 (1) (1987) 111–125.
- [85] W. Krakow, D.A. Smith, A high-resolution electron microscopy investigation of some low-angle and twin boundary structures, *Ultramicroscopy* 22 (1–4) (1987) 47–55.
- [86] F. Ernst, M.W. Finnis, D. Hofmann, T. Muschik, U. Schönberger, U. Wolf, M. Methfessel, Theoretical prediction and direct observation of the 9R structure in Ag, *Phys. Rev. Lett.* 69 (4) (1992) 620.
- [87] P. Gallagher, The influence of alloying, temperature, and related effects on the stacking fault energy, *Metallurgical Transactions* 1 (9) (1970) 2429–2461.
- [88] D. Medlin, G. Campbell, C.B. Carter, Stacking defects in the 9R phase at an incoherent twin boundary in copper, *Acta Mater.* 46 (14) (1998) 5135–5142.
- [89] Q. Li, S. Xue, J. Wang, S. Shao, A.H. Kwong, A. Giwa, Z. Fan, Y. Liu, Z. Qi, J. Ding, High-strength nanotwinned Al alloys with 9R phase, *Adv. Mater.* 30 (11) (2018) 1704629.
- [90] Y. Zhang, S. Xue, Q. Li, C. Fan, R. Su, J. Ding, H. Wang, H. Wang, X. Zhang, Microstructure and mechanical behavior of nanotwinned AlTi alloys with 9R phase, *Scripta Mater.* 148 (2018) 5–9.
- [91] S. Xue, Q. Li, Z. Fan, H. Wang, Y. Zhang, J. Ding, H. Wang, X. Zhang, Strengthening mechanisms and deformability of nanotwinned AlMg alloys, *J. Mater. Res.* 33 (22) (2018) 3739–3749.